# Fabrication of Microchannels Using Polynorbornene Photosensitive Sacrificial Materials

**Xiaoqun Wu,[a] Hollie A. Reed,[a] Yong Wang,[a] Larry F. Rhodes,[b] Ed Elce,[b] R. Ravikiran,[b] Robert A. Shick,[b] Clifford L. Henderson,[a] Sue Ann Bidstrup Allen,[a] and Paul A. Kohl[a,*,z]**

[a]*School of Chemical Engineering, Georgia Institute of Technology, Atlanta, Georgia 30332-0100, USA*
[b]*Promerus Limited Liability Company, Brecksville, Ohio 44141, USA*

A processing method has been demonstrated for the fabrication of microchannels using photosensitive polynorbornene copolymer based sacrificial materials. The channel geometric patterns of sacrificial polymer were made via photolithography. The sacrificial polymer patterns were encapsulated with a dielectric medium and then thermally decomposed to form air channels. For the thermal decomposition of sacrificial polymer, the heating program was determined on the basis of the kinetic model obtained from thermogravimetric analysis to maintain the decomposition at a constant rate. The results indicate that a properly selected heating program can avoid the deformation in the channel structure; at the same conditions, a large-size channel is more easily deformed than a small one. The tapered-structure microchannels were also produced using a gray-scale mask. The result shows that a suitably low contrast for the photosensitive sacrificial material can lead to smooth and tapered microchannels.
© 2003 The Electrochemical Society.   [DOI: 10.1149/1.1596955] All rights reserved.

Microfluidic devices have tremendous potential for applications in various fields including drug discovery, biomedical testing, and chemical synthesis and analysis. In such devices, liquids and gases are manipulated in microchannels with cross-sectional dimensions on the order of tens to hundreds of micrometers. Processing in such microchannel devices offers advantages including low reagent and analyte consumption, highly compact and portable systems, fast processing times, and the potential for disposable systems.[1-3] However, despite all their promise, microfluidic devices are currently being used in a limited number of applications and, generally, are simple devices in terms of their operational complexity and capabilities. For example, in terms of making truly portable microanalytical systems, one current difficulty involves the simple integration of electronic (*e.g.*, sensing methods) and fluidic elements into the same device. A most important issue, which controls this ability to integrate functions into the same device and thus controls the level of functionality of a microfluidic device is the method used to fabricate the structure.

The two most prevalent methods for fabricating microfluidic devices to date involve either bonding together layers of ultraflat glass or elastomeric polymers such as poly(dimethylsiloxane).[4] Both methods suffer from severe limitations and difficulties associated with integrating nonfluidic elements such as detectors with the microchannel system in the same substrate.[4-6] A method developed recently, which uses microchannel fabrication methods that are completely compatible with standard silicon complementary metal oxide semiconductor (CMOS) processes, can overcome many of these limitations and thus permit the integration of electronic control, actuation, and detection systems into a single device during the same fabrication sequence.[7] The first version of this method involves the use of a sacrificial polymer (polynorbornene) as a structural placeholder for channel formation using a conventional semiconductor process flow. The sacrificial polymer is first deposited as a blanket film by spin-casting or other deposition methods. A protective etch hard mask such as silicon dioxide is then coated onto the polymer layer and patterned using conventional photolithography and oxygen plasma etching. This patterned hard mask protects the underlying polymer from the etchant, leaving behind polymer relief patterns. These polymer structures are overcoated with a permanent structural material such as a polyimide or oxide. This sequence can be repeated to build up multilayer channel structures. Once all desired structures are formed, the entire device is heated to the decomposition temperature of the sacrificial polymer, leaving behind open microchannel structures.

This first sacrificial polymer fabrication method suffers from several limitations including that it requires on the order of ten processing steps to complete the sequence for a single level of microchannels. Recently, an improved sacrificial polymer method using photodefinable norbornene copolymers was reported which completely eliminates the need for hard mask deposition, photoresist patterning, and plasma etching. This improved method thus dramatically reduces the number of process steps required, resulting in a process that can be completed in only five steps (see Fig. 1).[8,9] In addition to significantly reducing the number of process steps required, this method also opens up the possibility of forming arbitrarily shaped, three-dimensional (3D) channel structures using gray-scale lithography as suggested in our prior publication.[9]

These photosensitive norbornene copolymer sacrificial materials consist of formulations of copolymers of pendant butyl- and alkenyl-substituted norbornenes (PNB) with small additions of a photoinitiator (PI) to selectively induce cross-linking. The photolithographic characteristics, photoinitiation systems, and thermal decomposition properties of these sacrificial materials have been investigated systematically in previous studies.[8,9] These experimental results provide the basic information required for the fabrication of microchannels using these sacrificial materials. However, it was shown in the work of Bhusari *et al.*,[7] that the cross-sectional shape of channel structures produced using these sacrificial polymer methods may be arched under certain processing conditions. This unintentional curvature was ascribed to possible flow of the overcoat medium during the relatively high temperature decomposition process. However, no further information was available at the time that could be used to guide process design to prevent this deformation in channel shape. The ability to prevent channel deformation is particularly important when the goal of the fabrication sequence is to build channels with controlled 3D cross-sectional shapes.

The main goal of this work is to further develop and demonstrate the use of photodefinable sacrificial polymer fabrication methods to produce channel geometries with arbitrarily shaped cross-sectional profiles. This ability to control the shape of the channel cross section is expected to be particularly useful in precisely controlling the flow of fluids in microchannel systems. The ability to control fluid flow patterns and dispersion by controlling the channel cross section is investigated through computational fluid dynamics simulations. Tapered cross-sectional channel profiles are useful in preserving ''plug flow'' conditions in curved microchannels and thus reducing dispersion of components in the flow. Therefore, the thermal decomposi-
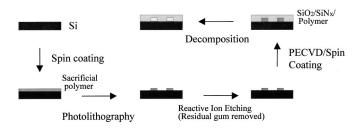
**Figure 1.** Schematic of processing steps for microchannel fabrication using photodefinable polymer sacrificial materials.



**Figure 2.** Schematic of microchannel cross sections simulated using Fluent.
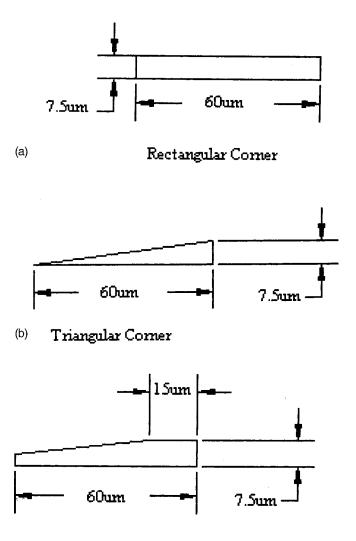
tion of the photodefinable sacrificial polymers was studied in detail and novel heating protocols were developed that maintain the channel shape during decomposition. The use of these methods is finally demonstrated using gray-scale lithography to produce microchannels with tapered cross sections.

**Simulation of Flow in Curved Channels**

When designing and fabricating microfluidic devices, it is almost inevitable that channels with curved shapes are required. For example, when designing a long separation column on a chip, turning the channel into a meandering path may be required to keep the device within some required size limits. In such cases, it can be extremely important to precisely control the fluid flow pattern in the channel so as to minimize differences in the residence time distribution of fluid traveling through the channel. Generally, maintaining near plug flow conditions in devices used for separations, analysis, and other fluidic operations prevents mixing and loss of spatial confinement of fluid samples after injection or separation. One particular problem is minimizing residence time variations for fluids traveling through corners and curved sections of microfluidic channels. To illustrate this point and investigate the improvements that could be realized by using channels with tapered cross sections, a series of computational fluid dynamics simulations were performed.

Fluent, a computational fluid dynamics (CFD) simulation package produced by Fluent Inc., was used to simulate the flow in a series of different corner designs for microchannels. GAMBIT, a preprocessor accessory for FLUENT made by Fluent Inc., was used to construct the desired model geometry, apply the meshing points to the model, and define the required boundary zones. Once defined, Fluent was used to simulate the flow pattern in each microchannel and to produce numerical and graphical results for each case.

In this work, a series of 90° turns in microchannels were simulated with varying cross-sectional geometries. Figure 2 shows the cross sections of the four simulated channels. Figure 2a shows the dimensions of a uniform area channel. Figures 2b and c show channels with tapered corners. The taper improved the flow around corners with Fig. 2c representing a near optimized design. The inside radius of the turns was held constant at 60 μm and the outside radius of the turns was held constant at 120 μm. The same boundary conditions were applied in simulating the flow through these channels and a constant pressure outlet condition which was assumed to be atmospheric pressure. In this case, water was used as the flow media, but the results should be general to any Newtonian fluid under laminar flow conditions. Under these conditions, the flow rates and Reynolds numbers are low which indicate laminar flow conditions, and thus a laminar flow model was used in Fluent for solution of these problems. To look at the dispersion which occurs in fluid flowing around each of these microchannel corners, fluid packet trajectories and transit times around each turn were calculated. Figure 3 shows plots of the transit times for fluid packets as a function of radial distance along the corner for each type of turn structure. The appearance of different lines of packet transit times on these plots are due to the fluid packets at different vertical positions within the channels also experiencing slight dispersion due to low velocities near the top and bottom surfaces of the channel.

Figure 3a clearly shows that the standard rectangular channel geometry results in severe dispersion of an initially flat concentration profile after traveling around the 90° turn. Under laminar flow conditions, the relatively uniform velocity profile across the channel cross section coupled with the longer path length for fluid at the outside of the turn result in transit times which are a factor of 3 to 5 larger for fluid at the outside radius as compared to fluid at the inside radius. This dispersion would be even more exaggerated for a 180° bend. One natural solution to this problem is to decrease the velocity of the fluid near the inside radius of the turn to achieve equal transit times for the fluid regardless of radial position. One way to achieve this velocity modification is to alter the cross-sectional area of different regions of the channel. Figure 3b shows the transit time profile for fluid flowing around a turn in a triangular cross section channel. The reduced channel height at the inside radius of the turn is expected to slow the velocity of fluid along the inside of the turn. Figure 3b shows that the triangular cross section overcompensates and results in longer transit times for fluid near the inside radius as compared to fluid near the outside radius. From close inspection of the Fluent results, it is also apparent that channel sections which have two walls intersecting at acute angles lead to significant dispersion in these regions, and thus acute angles in the channel cross section geometry should be avoided if possible. Based on these facts, an optimization was performed to design an improved channel cross section profile that would result in minimal dispersion around
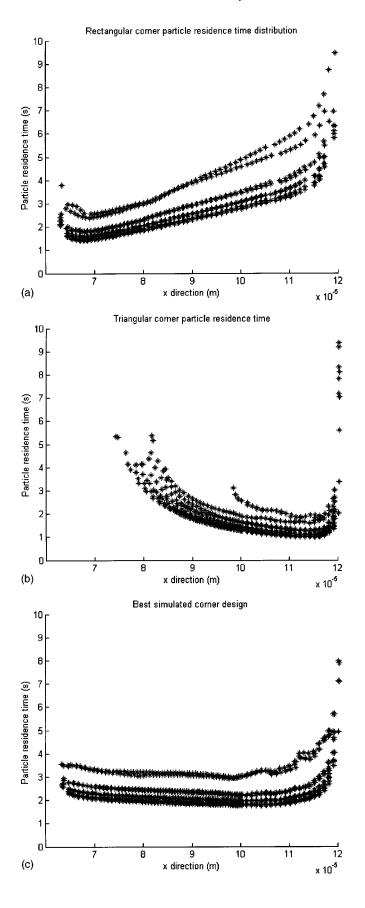
**Figure 3.** Fluid transit time plots for flow around 90° turns with 60 μm inside radii for microchannel cross sections shown in Fig. 2, (a) corresponds to Fig. 2a, (b) corresponds to Fig. 2b, and (c) corresponds to Fig. 2c.

the simulated turn. Figure 3c shows the fluid transit time results for such an improved channel structure. The transit time profile is essentially uniform for fluid flowing around a 90° corner using this improved shape. Thus, it is clear that by designing the cross-sectional shape of microchannels in turns it should be possible to minimize dispersion in the flow profiles.

## Experimental

The sacrificial polymer used in this work was Unity 4481P, which consists of the copolymer of 5-butyl norbornene (BuNB) and 5-alkenyl norbornene (ANB) in the molar ratio 73/27 (Promerus LLC, Brecksville, OH). The polymer weight average molecular weight ($M_w$) and polydispersity index (PDI) were measured to be 425,000 and 3.74 respectively by gel permeation chromatography using polystyrene calibration standards. Bis(2,4,6-trimethylbenzoyl)-phenylphosphineoxide (Irgacure 819, Ciba Specialty Chemicals Inc.) was used as a free radical photoinitiator (PI) for this work. Solutions of PNB and PI were prepared using mesitylene (MS, 97%, Aldrich) as the solvent. Two different formulations, PNB/PI/MS in a mole ratio of 16/0.32/84 (2 wt % initiator relative to dry polymer) and PNB/PI/MS in a mole ratio of 16/0.64/84 (4 wt % initiator relative to dry polymer) (weight ratios), were used in the experiments. After exposure and baking, polymer patterns were developed using xylene ( > 98.5 + %, Aldrich).

Thermal decomposition characteristics of the sacrificial polymer were investigated using a Seiko Instruments Inc. TG/DTA 320 system. Thermogravimetric analysis (TGA) measurements were performed under $N_2$ at a purge rate of 28 mL/min. The encapsulated sacrificial polymer structures were thermally decomposed in a Lindberg tube furnace purged with $N_2$.

For microchannel fabrication, PNB/PI films were cast onto silicon wafers using a Brewer Science CEE 100 spinner and hot plate system. A 3.5-4.0 μm thick PNB/PI film was obtained at a spin speed of 2400 rpm and a softbake of 110°C for 60 s. Film thicknesses were measured using a Veeco Dektak profilometer. An OAI mask aligner equipped with an *i*-line filtered UV irradiation source (365 nm wavelength) was used to expose and pattern the PNB/PI films. Before exposure, the intensity of UV light source was measured using an OAI model 356 exposure analyzer with a 365 nm probe. After exposure, samples were postexposure baked at 120°C for 30 min in an oven. Samples were developed using a continuous spray of xylene while the wafer was spun at 500 rpm.

Removal of any polymer residue from the developed patterns was accomplished using a PlasmaTherm reactive ion etching (RIE) system using the following conditions: 5 sccm $CHF_3$, 45 sccm $O_2$, 250 mTorr, 300 W, 35°C. The etching rate of the polymer under these conditions is approximately 300 nm/min. Plasma enhanced chemical vapor deposition (PECVD) was performed to deposit an $SiO_2$ overcoat for encapsulation of the polymer channel patterns. The $SiO_2$ was deposited with a PlasmaTherm PECVD using the following conditions: 380 kHz rf frequency, 50 W power, 200°C, 550 mTorr, and a gas mixture of $N_2O$ (1400 sccm) and 2% $SiH_4$ diluted in $N_2$ (400 sccm). The deposition rate for the oxide using these conditions is approximately 50 nm/min.

*Thermal decomposition program.*—For the thermal decomposition process, the fractional decomposition can be calculated from the TG curve as shown in Eq. 1

$$\alpha = \frac{W_0 - W}{W_0 - W_f} \quad [1]$$

where $W_0$ is the initial mass, $W$ is the mass remaining at some time during the decomposition, and $W_f$ is the final mass of the sample at the end of the thermal cycle. The kinetic description for thermal decomposition of the polymer is generally expressed as

$$\frac{d\alpha}{dt} = k(1 - \alpha)^n = A \exp\left(-\frac{E_a}{RT}\right)(1 - \alpha)^n \quad [2]$$

where $n$ is the overall order of decomposition reaction, $A$ is the Arrhenius pre-exponential factor, and $E_a$ is the activation energy of the decomposition reaction.

To avoid a sudden and large release of the gaseous decomposition products from the polymer patterns that may result in distortion of the channel structure, it is desired to keep the decomposition rate ($d\alpha/dt$) constant during the entire decomposition process. Assuming the decomposition rate is equal to a constant, $r$, throughout the decomposition process then

$$\frac{d\alpha}{dt} = r, \text{ and } t = 0, \ \alpha = 0 \qquad [3]$$

Integrating Eq. 3 gives the general desired result shown in

$$\alpha = rt \qquad [4]$$

Assuming that the reaction order, activation energy, and pre-exponential factor do not change significantly during the decomposition, $d\alpha/dt$ and $\alpha$ can be replaced with $r$ and $rt$, respectively, in Eq. 2 which results in the following equation

$$r = A \exp\left(-\frac{E_a}{RT}\right)(1 - rt)^n \qquad [5]$$

It is now possible to rearrange Eq. 5 to solve for the necessary temperature *vs.* time profile that is required to maintain a constant rate of polymer decomposition throughout the entire process. The explicit expression for temperature *vs.* time is shown in

$$T = \frac{E_a}{R}\left[\ln\frac{A(1 - rt)^n}{r}\right]^{-1} \qquad [6]$$

Thus, to design a heating profile it is necessary to specify four parameters: the three kinetic parameters ($A$, $E_a$, and $n$) that describe the polymer decomposition, and $r$ the desired polymer decomposition rate. Based on regression of TGA data performed in previous experiments,[9] the kinetic parameters for the polymer used here were determined to be $A = 5.8 \times 10^{14}$ min$^{-1}$, $E_a = 207$ kJ/mol, and $n = 1.05$. Thus, for a given constant decomposition rate, $r$, one can obtain a curve of temperature *vs.* decomposition time.

## Results and Discussion

*Decomposition condition.*—Thermal decomposition of the sacrificial polymer was performed in a pure nitrogen atmosphere to avoid any oxidation of the polymer that could result in the formation of nonvolatile decomposition products and undesirable residue in the microchannels. In addition to using an inert atmosphere, as suggested previously, a controlled heating profile was used to maintain a relatively constant polymer decomposition rate. This constant decomposition rate ensures that gaseous products are not released so quickly that pressures high enough to significantly deform the channel shape are generated.

Figure 4 shows curves of the decomposition rate *vs.* time for pure PNB samples decomposed at both a constant 425°C (isothermal decomposition) and various heating rates (dynamic decomposition), respectively. In each case, there is a peak in the decomposition rate. The width of the peak corresponds to the transition period during the conversion of sacrificial polymer to gaseous products. Higher heating rates or high temperature isothermal decompositions result in a sharp peak in the decomposition rate profile. This implies that the majority of the decomposition process occurs over a short time interval, thus resulting in a sudden and large release of the gaseous decomposition products. It was therefore expected that controlling the decomposition rate at a constant low level using controlled heating profiles could eliminate this phenomenon and thus prevent channel distortion during decomposition. It was decided to test this
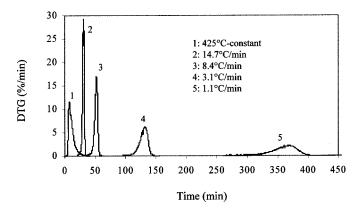
**Figure 4.** DTG curves for pure PNB samples decomposed at a constant 425°C (isothermal decomposition) or various heating rates (dynamic decomposition).

theory by comparing the effect of various decomposition procedures on the final resulting microchannel shapes and sizes.

Based on Eq. 6, the temperature *vs.* time heating profiles required to achieve decomposition rates of 1, 2, and 3%/min were calculated and are shown in Fig. 5. Figure 5 illustrates that, at a constant decomposition rate, the decomposition temperature during most of decomposition time should be set relatively low with a slight ramp rate. However as the decomposition nears completion, higher temperatures can be used which help obtain complete decomposition of the polymer within a reasonable time.

Representative temperature profiles that closely approximate the smooth temperature *vs.* time curves produced using Eq. 6 were used to perform the decompositions. Figure 6 shows the temperature *vs.* time curve calculated using Eq. 6 and the corresponding simple mimic heating profile that was tested in the Lindberg decomposition furnaces for device fabrication. Figure 7 shows TGA results for the simple mimic heating program that was designed to achieve a 1%/min decomposition rate. The DTG curve demonstrates that the decomposition rate does fluctuate closely around the desired 1%/min level without extreme variations. Thus, the sharp peak in the decomposition rate shown in Fig. 4 can be avoided by using more intelligent heating profiles. When this same heating profile is used in processing encapsulated polymer samples, no distortion in the encapsulated channels was observed but electron microscopy revealed that small amounts of polymer residue were left in the channel structures. Two different modifications to the mimic heating profile were tested in an attempt to remove this residual polymer. In the first case, a final hold at 455°C for 1 h was used in an attempt to remove the
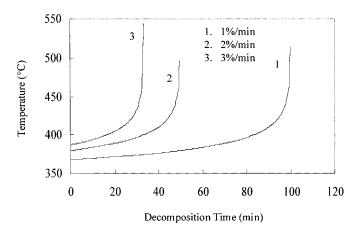
**Figure 5.** Calculated trends of temperature *vs.* time for the decomposition of pure polymer at rates of 1, 2, and 3%/min.
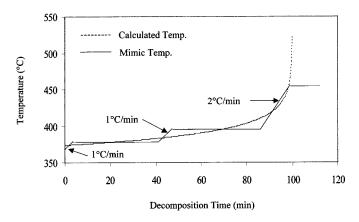
**Figure 6.** Calculated and mimic heating programs for the decomposition of pure polymer at a rate of 1%/min.

residual polymer. This high temperature hold did reduce the residual remaining polymer substantially as observed in scanning electron microscopy (SEM) cross sections, but some remaining residue was left even after the 1 h hold. A second method which involved doubling the intermediate holds shown in Fig. 6 was also tested. This effectively reduced the average decomposition rate even further approaching the 0.5%/min level. In this case, it was observed that no distortion of the channel profile occurred during the decomposition and essentially no polymer residue was found in the microchannel after decomposition. This suggests that there may be additional byproducts formed during the decomposition if the process is ramped too quickly which result in a residue that can be difficult to remove with even high temperature processing. Longer holds at lower temperatures can be used to both slow the decomposition rate and thus reduce pattern profile distortion and to eliminate residual polymer in the final channel structures.

*Microchannels encapsulated with polyimide and* $SiO_2$.—Microchannels have been made following the scheme in Fig. 1. In the processing, a 3.5-4.0 $\mu$m thick PNB/PI film (4 wt % initiator in PNB) was cast using a spin speed of 2400 rpm and softbake condition of 110°C/60 s. The film was exposed to UV light using a chrome on quartz mask with dose of 450 mJ/cm$^2$ and postexposure baked at 120°C for 30 min in an oven. After postexposure baking, the film was spray developed using xylene to produce the desired channel patterns. There was no noticeable residue remaining after development in the patterned areas, but direct overcoating of the encapsulant material on the as-developed features resulted in poor adhesion to the substrate. Small bubbles formed in the overcoat materials in the areas where the sacrificial polymer was presumably
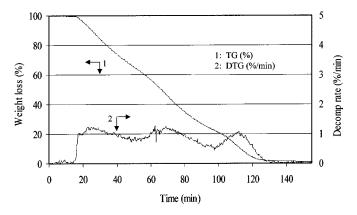


**Figure 7.** TGA results for the mimic heating program set for a nominal decomposition rate of 1%/min.
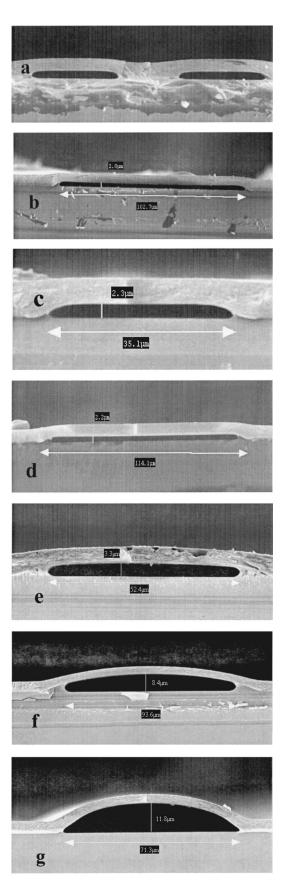


**Figure 8.** SEM images of the channels encapsulated with polyimide and decomposed with at rates of (a, b) 1%/min, (c, d) 2%/min, (e, f) 3%/min, and (g) at a constant 425°C.

developed cleanly away from the substrate. Therefore, it was concluded that there must be a small amount of remaining polymer residue after development that prevents good adhesion of the overcoat to the substrate. To avoid this phenomenon, a residue removal treatment was employed by dry etching in an oxygen plasma using an RIE before the channel patterns are encapsulated. After residue removal using the plasma, samples were then encapsulated using either polyimide or $SiO_2$. Polyimides are good materials for encapsulation because they display high glass transition temperatures and thermal stability, low dielectric constant, modulus, moisture adsorption, and stress.[7] In this work, HD Microsystems PI 2734 polyimide, was used to overcoat some channel structures. In these cases, the PI 2734 was spin-coated on the top of the channel patterns at a speed of 2300 rpm for 30 s, and cured at 350°C for 1 h under $N_2$. The thickness of the polyimide layer under these conditions is approximately 4.5 μm. In addition, some channel structures were encapsulated using $SiO_2$. In these cases, a 2 μm thick encapsulation layer of $SiO_2$ was deposited using the PECVD recipe described earlier.

The decomposition of the encapsulated polymer patterns was performed at various decomposition rates to investigate the effect of the rate on the channel structure. Figures 8a through g show SEM images of the channel encapsulated with polyimide and decomposed at different rates using different heating profiles. The results indicate that the decomposition rate does affect the channel structure significantly. At low decomposition rates (1 or 2%/min), the channel structures produced maintain the size and shape of the original PNB sacrificial polymer pattern. However, at relatively high decomposition rates (3%/min) or when a high constant temperature decomposition process is used, the microchannels are distorted into dome or arc shaped profiles. It is also obvious that this distortion problem becomes a more important issue for microchannels as their lateral size increases. Channels with larger widths clearly deformed more than channels of smaller dimensions. SEM images of channels encapsulated with $SiO_2$ are shown in Fig. 9a-f. It was observed that the extent of channel deformation appears to be higher in the $SiO_2$ overcoated structures as compared to the polyimide overcoated channels at the same nominal channel feature sizes and polymer decomposition rates. This larger deformation in the $SiO_2$ overcoated samples could be due to both differences in the mechanical properties of the two overcoat materials and differences in the diffusion rate of the decomposition products through the overcoat materials.

*Microchannels with tapered cross-sectional structure.*—As discussed previously, one goal of this work was to provide a simple fabrication method for microchannels with tapered cross-sectional profiles that could be used to control fluid flow patterns in microchannels. To fabricate the tapered microchannel structures, the concept described here is to use a lithography process employing a gray-scale photomask and a low contrast photosensitive sacrificial material. A series of experiments was performed to investigate the possibility of using such an approach for producing microchannels that are shaped in a controlled manner in all three dimensions.

Channel features were designed with an approximately linear gradient in percent transmission across the width of the channel with varying ratios of chrome stripes to clear transparent area. In this particular case, the chrome stripe features were designed to be 200 nm in size and thus served as subresolution features for the photosensitive sacrificial polymers used. Two masks were fabricated from these designs by electron beam lithography at ETEC Systems (Hayward, CA). Table I describes the two main channel features used in more detail. Using this type of gray-scale mask allows for the photosensitive sacrificial material to be exposed to a range of doses across the width of the channel feature using a single lithographic exposure step. This exposure gradient in conjunction with a low contrast resist material can be used to produce a feature that is shaped in both the lateral and vertical directions with respect to the plane of the substrate in a single lithographic process. Two photosensitive materials with different contrast levels were used to generate tapered microchannel structures with this mask. Figure 10
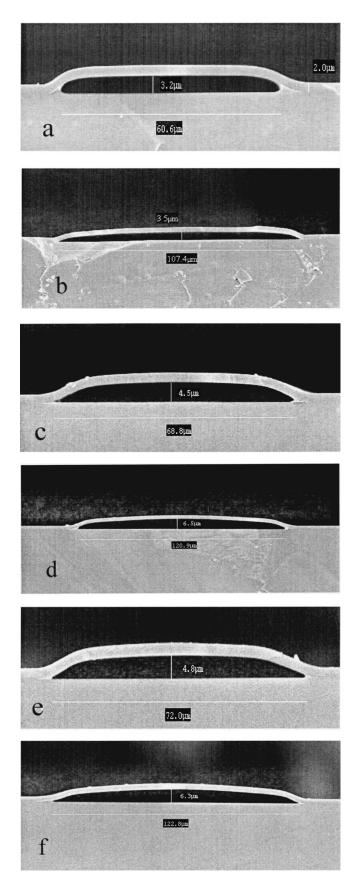


**Figure 9.** Microchannels encapsulated with $SiO_2$ and decomposed at rates of (a, b) 0.5, (c, d) 1, and (e, f) 3%/min.

**Table I. Characteristics of the gray-scale microchannel photomask.**

Feature I
| | |
|---|---|
| Channel width (μm) | 60 |
| Zone size (μm) | 6 6 6 ................. 6 6 6 |
| Transparency (TP) (%) | 100 90 80 ............... 30 20 10 |

Feature II
| | |
|---|---|
| Channel width (μm) | 80 |
| Zone size (μm) | 4 4 4 ................. 4 4 4 |
| Transparency (TP) (%) | 100 95 90 ................... 15 10 5 |

shows the contrast curves for the two photosensitive sacrificial polymer formulations. The methods of measuring contrast curves and calculating contrast values for these materials have been discussed previously in the literature.[8,9] The contrast factors for these two systems are a modest 0.51 and 0.85 for the 2 wt % (referred to as material 1) and 4 wt % (referred to as material 2) photoinitiator relative to dry polymer loadings, respectively.

Using this contrast curve data, it is possible to quickly calculate a rough prediction of the pattern profile that results from exposure using a gray-scale mask with these photosensitive materials if the relative transparency as a function of position on the mask is known accurately. Based on polynomial fitting, the contrast curves can be adequately described using the following functions

$$f_1 = 0.0236[\log(D)]^3 - 0.357[\log(D)]^2 + 1.818[\log(D)] - 2.13 \qquad [7]$$

$$f_2 = 0.0352[\log(D)]^3 - 0.653[\log(D)]^2 + 2.95[\log(D)] - 2.92 \qquad [8]$$

Here $f_i$ is the fraction of the film thickness remaining after exposure to a dose $D$ and wet development for material i.

An approximate shape of the channel patterns that may be produced from a gray-scale mask can thus be predicted using Eq. 9

$$d(x) = f_i(\log[D \cdot TP(x)]) \cdot FT \qquad [9]$$

where, $f_i$ is the contrast function for material i, $d(x)$ is the thickness of the film (after development) at a certain position $x$ across the channel pattern, $TP(x)$ is the fractional transparency of the mask at position $x$ across the feature, $D$ is the nominal exposure dose used, and $FT$ is the original thickness of the cast film. The outline of the simulated channel pattern consists of the points calculated by Eq. 9, which were then smoothed by seven-point smoothing
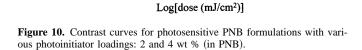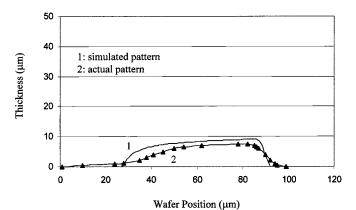


**Figure 11.** Real and simulated channel patterns (with feature I of the mask) for the system with 2 wt % initiator loading.

$$S_i = \frac{Y_{i-3} + 2Y_{i-2} + 3Y_{i-1} + 4Y_i + 3Y_{i+1} + 2Y_{i+2} + Y_{i+3}}{16}$$

$$[10]$$

where $S_i$ and $Y_i$ are the smoothed signal and original signal for the $i$th point, respectively.

Tapered-structure channel patterns were fabricated using the gray-scale lithographic approach using a sequence of steps similar to those outlined in Fig. 1. First, 12 μm thick PNB/PI films were cast using a spin speed of 700 rpm and softbake condition of 110°C for 2 min. The films were then exposed to UV light with the gray-scale mask. The nominal exposure dose was set using the contrast curve data for the photosensitive material to obtain a film with 80% original thickness remaining after development under a 100% transparent feature. The doses used were 1300 and 165 mJ/cm² for 2 and 4 wt % initiator loadings, respectively. The films were postexposure baked at 120°C for 30 min in oven. The films were spray developed using xylene at a spin speed of 500 rpm for 30 s. The final shape of the microchannel patterns was measured using profilometry.

Figures 11 and 12 show the real feature I type PNB patterns produced as measured by profilometry, and for comparison the predicted microchannel patterns (using Eq. 7 through 10), for the systems with 2 and 4 wt % initiator loadings. A comparison between different patterns produced by the two formulations clearly shows that the material with the lower contrast produces a profile that more closely resembles the desired smoothly tapered structure. However, it can be seen that the simple prediction of the profile shape only roughly approximates the actual feature produced using this method.
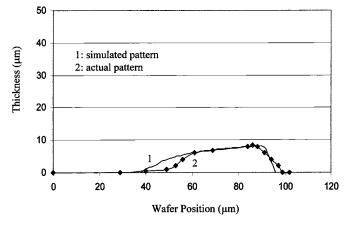


**Figure 10.** Contrast curves for photosensitive PNB formulations with various photoinitiator loadings: 2 and 4 wt % (in PNB).



**Figure 12.** Real and simulated channel patterns (with feature I of the mask) for the system with 4 wt % initiator loading.
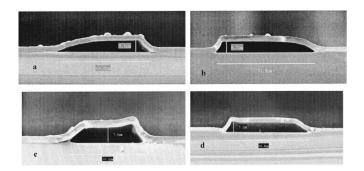
**Figure 13.** SEM images of tapered microchannels made by using (a) feature I of the gray-scale mask with 2% PI, (b) feature II with 2% PI, (c) feature I with 4% PI, and (d) feature II with 4% PI.

Upon closer inspection of the mask, it was apparent that the desired smooth gradient in transmission was not faithfully reproduced into the mask due to the extremely small feature sizes used for the constituent patterns. This brings up the issue that accurate gray-scale mask production for such a method may be a challenging task. In any case, with more careful attention and accurate transfer of the design to the mask, it should be possible to use the contrast data for a material in conjunction with Eq. 7 through 10 to design a gray-scale mask feature for a specific photosensitive material that can be used in principle to obtain any desired pattern shape.

The tapered polymer microchannel patterns were next overcoated and decomposed to test the ability to transfer the tapered profile into the final microchannel. First, any polymer residue was removed from the substrate using an oxygen RIE plasma etch. The channel patterns were then encapsulated with $SiO_2$ using the same conditions described previously. The thermal decomposition of encapsulated channel patterns was performed under $N_2$ with a decomposition rate of 0.5%/min. SEM images of the resulting tapered microchannels are shown in Fig. 13a-d. Due to the ability to carefully control the decomposition rate of the polymer by controlling the heating profile during decomposition, no deformation was observed in the channel structure. This can be seen by comparing the profiles of the original PNB patterns in Fig. 11 and 12 with the SEM channel cross sections in Fig. 13. The widths of the channels in Fig.
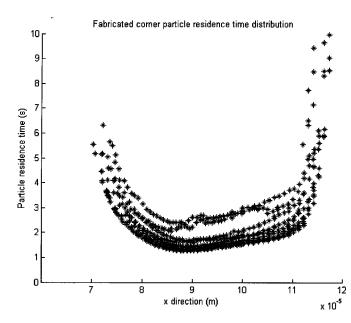
13c and d are narrower than the feature sizes on the gray-scale mask due in part to slight RIE overetching during the polymer residue removal step. Comparing Fig. 13a and b with Fig. 13c and d, it can be seen that a low contrast sacrificial material is desirable for the fabrication of smoothly tapered microchannel structures. The right side of Fig. 13a and c, and the left side of Fig. 13b and d are nongray-scale features, for reference. As expected, the final shape of the channel structure is determined by a combination of the gray-scale pattern on the mask, the contrast of the photosensitive material, and the nominal exposure dose used in printing the feature.

To obtain an idea of the effectiveness of fabricated channel cross sections in reducing dispersion in flow around microchannel corners, the expected fluid transit times around a corner of the shape shown in Fig. 11a were simulated using Fluent as described previously. Figure 14 shows the predicted transit times for flow around this corner using the boundary conditions and velocities used in the earlier idealized channel simulations. It is clear from this simulation that even the crudely shaped channel fabricated for demonstration is expected to perform better than the standard rectangular cross section channel. Further, it is hoped that by optimizing mask design and process conditions, a more ideal shape similar to that shown in Fig. 3c can be achieved and used for device fabrication. This further refinement of the process is the subject of ongoing work.

## Conclusions

The fabrication of microchannels has been demonstrated using photosensitive sacrificial polymer materials. The process consists of patterning the sacrificial polymer via photolithography, removal of polymer residue using RIE, encapsulation with a dielectric medium, and thermal decomposition of encapsulated polymer channel patterns. A method for designing heating programs to keep the thermal decomposition of sacrificial polymer at a constant rate was presented using the kinetic model of polymer decomposition. Heating programs designed using this approach have been demonstrated to prevent sudden and large decomposition rates (*i.e.*, which result in rapid release of gaseous decomposition products that distort channel features), and were also shown to produce microchannel patterns with well-controlled shapes that do not exhibit any substantial deformation after the thermal decomposition of the sacrificial polymer. Controlling the decomposition rate and slowly releasing the gaseous decomposition products allows the decomposition products to permeate through the overcoat at a rate roughly equivalent to the decomposition rate, and thus avoids the buildup of large pressures in the microchannel which can lead to distortion and failure of the structure. It was also found that larger channels have a higher tendency toward distortion. A gray-scale lithographic process has been developed and demonstrated for the production of microchannels with tapered cross sections. Such tapered channels have been shown through simulation to be able to reduce effects such as dispersion that are detrimental to microfluidic system performance.

**Figure 14.** Fluent simulation of fluid transit times around 90° corner with 60 μm inside radius for microchannel with cross section similar to that shown in Fig. 11(1).

## References

1. J. C. McDonald, D. C. Duffy, J. R. Anderson, D. T. Chiu, H. Wu, O. J. A. Schueller, and G. M. Whitesides, *Electrophoresis,* **21**, 27 (2000).
2. V. Dolnik, S. Liu, and S. Jovanovich, *Electrophoresis,* **21**, 41 (2000).
3. M. Koch, A. Evans, and A. Brunnschweiler, *Microfluidic Technology and Applications*, Chap. 6 and 7, American Technical Publishers Ltd. (Hertfordshire, U.K., 2000).
4. N. F. Raley, J. C. Davidson, and J. W. Balch, *Proc. SPIE,* **3224**, 185 (1997).

5. N. F. Raley, J. C. Davidson, and J. W. Balch, *Proc. SPIE,* **2639**, 40 (1998).
6. P. Pethig, J. P. H. Burt, A. Parton, N. Rizvi, M. S. Talary, and J. A. Tame, *J. Micromech. Microeng.,* **8**, 356 (1998).
7. D. Bhusari, H. Reed, M. Wedlake, A. Padovani, S. A. Bidstrup-Allen, and P. Kohl, *J. Microelectromech. Syst.,* **10**, 400 (2001).

8. X. Q. Wu, H. A. Reed, L. F. Rhodes, E. Elce, R. Ravikiran, R. A. Shick, C. L. Henderson, S. A. Bidstrup Allen, and P. A. Kohl, *J. Electrochem. Soc.,* **149**, G555 (2002).
9. X. Q. Wu, H. A. Reed, L. F. Rhodes, E. Elce, R. Ravikiran, R. A. Shick, C. L. Henderson, S. A. Bidstrup Allen, and P. A. Kohl, *J. Appl. Polym. Sci.*, In press.